Geophysical Research Letters

RESEARCH LETTER
10.1029/2025GL120156

Precipitation Response to Mesoscale SST Variability: Insights From Observations and Multi-Resolution Models

Xiaoqi Wang[1], R. Justin Small[2], Ping Chang[1], Meng Lyu[1], and Dan Fu[1]

[1]Department of Oceanography, Texas A&M University, College Station, Texas, USA, [2]Climate and Global Dynamics Laboratory, NSF National Center for Atmospheric Research, Boulder, CO, USA

Key Points:

- Satellite observations, ERA5 reanalysis and high-resolution models capture a precipitation response to mesoscale SST variability that is missing in low-resolution models
- A vertical velocity response extending up to 500 hPa is observed in both ERA5 and high-resolution models
- Precipitation response to mesoscale SST variability in climate models and reanalysis is primarily due to parameterized convective component

Supporting Information:

Supporting Information may be found in the online version of this article.

Correspondence to:

X. Wang and M. Lyu,
cinky77@tamu.edu;
mengmeng92@tamu.edu

Citation:

Wang, X., Small, R. J., Chang, P., Lyu, M., & Fu, D. (2026). Precipitation response to mesoscale SST variability: Insights from observations and multi-resolution models. *Geophysical Research Letters*, *53*, e2025GL120156. https://doi.org/10.1029/2025GL120156

Received 20 OCT 2025
Accepted 11 JAN 2026

Author Contributions:

Conceptualization: Xiaoqi Wang, Ping Chang
Data curation: Xiaoqi Wang, Dan Fu
Formal analysis: Xiaoqi Wang, R. Justin Small, Meng Lyu
Funding acquisition: Ping Chang
Investigation: Xiaoqi Wang
Methodology: Xiaoqi Wang, Meng Lyu
Project administration: Ping Chang
Resources: Xiaoqi Wang
Software: Xiaoqi Wang, Meng Lyu
Supervision: R. Justin Small, Ping Chang
Validation: Xiaoqi Wang
Visualization: Xiaoqi Wang
Writing – original draft: Xiaoqi Wang

Abstract Mesoscale sea surface temperature (SST) variability influences the marine atmosphere boundary layer (MABL), affecting near-surface winds and turbulent heat fluxes. This study examines precipitation response to mesoscale SST forcing using satellite observations, ERA5 reanalysis, and high- and low-resolution climate models. The results show that high-resolution models produce a precipitation response to mesoscale SST consistent with satellite observations and ERA5. However, partitioning ERA5 and model precipitation into resolved and parameterized convective components reveals that even in high-resolution models, the simulated mesoscale SST-precipitation relationship is shaped by the characteristics of convective parameterization. Further, the precipitation response to SST is strongly dependent on the background SST and SST variability in coupled models. Further analysis of ERA5 and high-resolution simulations shows a vertical velocity response extending to 500 hPa. However, the reliance on convective parameterizations introduces uncertainties about whether high-resolution models accurately capture these effects.

Plain Language Summary Precipitation, a major feature of the Earth's climate, responds to large-scale (1,000s of km) changes of the atmosphere driven by ocean surface temperature fluctuations, such as in El Niño-Southern Oscillation events. However, the response to smaller-scale (10–100s of km) modulations of sea surface temperature (SST) is less well-known. For models of the Earth's climate, it is important to properly represent precipitation and its relation to SST, as precipitation leads to atmospheric heating and possible remote impacts on weather patterns. However, many key precipitation processes, such as cloud formation and atmospheric convection, occur at spatial scales smaller than typical climate model grid cells. Consequently, convective precipitation is approximated using parameterizations based on directly simulated larger-scale conditions. In this study, using a combination of observational data, historical weather reconstructions (known as reanalysis), and climate models with a range of different grid sizes, we examine how the models represent the precipitation response to mesoscale SST variations. Our analysis reveals that although state-of-the-art climate models with fine grids of 10–50 km can reproduce a precipitation response to mesoscale SST, the simulated precipitation depends on convective parameterizations and the magnitude of the response varies from model to model. This highlights uncertainties regarding whether these models accurately capture the atmospheric response to mesoscale SST.

1. Introduction

Embedded within the complex dynamics of Earth's climate system, precipitation—a major outcome of atmospheric convection—is a crucial ingredient of climate variability. Deep convection events perturb the background atmospheric state, potentially triggering teleconnections to remote regions via Rossby waves (Alexander et al., 2002; Horel & Wallace, 1981; Hoskins & Karoly, 1981). In turn, convection is modified by sea surface temperature (SST) patterns which can influence the stability of the atmospheric column and cause near-surface flow convergences (Gill & Rasmusson, 1983; Lindzen & Nigam, 1987; Matsuno, 1966). Possible feedbacks of convection onto near-surface flow are also important (Gill & Rasmusson, 1983). These processes vary regionally and across different spatial and temporal scales (Seager et al., 2010; Xie, 2004).

Here, we examine the effects of mesoscale SST anomalies on atmospheric processes at monthly timescales. Mesoscale SST variability, associated with oceanic mesoscale eddies and fronts, typically evolves on timescales of several weeks to months and is most pronounced along Western Boundary Currents (WBCs, e.g. the Gulf Stream, Kuroshio and Agulhas Currents), their eastward extensions, and the Antarctic Circumpolar Current (ACC) (Chelton & Xie, 2010). The WBCs are associated with temperature fronts between the warm subtropical

Writing – review & editing:
Xiaoqi Wang, R. Justin Small, Ping Chang, Meng Lyu, Dan Fu

waters and cooler waters poleward or inshore of the front. Instability of the flows leads to meanders and eddy generation (Cronin & Watts, 1996) and anomalies of SST which can reach up to several °C (Marshall et al., 2009). The distinctive mesoscale SST patterns modify wind stress and heat fluxes, subsequently triggering localized responses within the marine atmospheric boundary layer (MABL) (Chelton & Xie, 2010; Kelly et al., 2010; Kwon et al., 1998; O'Neill et al., 2005; Schneider, 2020; Seo et al., 2023; Small et al., 2008; Xie, 2004).

The effect of climatological WBCs and ocean fronts on the overlying atmosphere has been well studied and shown to include deep vertical motion and associated enhanced precipitation, and strengthening or shifting of storm tracks (Kuwano-Yoshida & Minobe, 2017; Minobe et al., 2008; Nakamura et al., 2004; Small et al., 2014; Taguchi et al., 2009; Woollings et al., 2010). The effect of mesoscale ocean variability on the free troposphere is less well-known, but it has been established that the precipitation response to composited mesoscale eddies is on average ~0.2 mm day^{-1} °C^{-1} from satellite and reanalysis data (Frenger et al., 2013), with regional and seasonal variations, and differing responses to warm versus cold SST anomalies (Liu et al., 2018). Larson et al. (2024) recently further identified statistically significant covariances between mesoscale precipitation and SST variability inherently resolved in Western Boundary Currents using monthly high-spatial-resolution SST data sets ($0.1° \times 0.1°$), a result that is consistent with stochastic climate models forced by both ocean noise (i.e., mesoscale variability) and atmosphere noise (i.e., weather variability) (Bishop et al., 2017; Wu et al., 2006). The influence of a field of oceanic mesoscale eddies on large-scale storm tracks and atmospheric rivers has also been demonstrated (Foussard et al., 2019; Liu et al., 2021; Ma et al., 2015, 2017).

Precipitation in the midlatitude regions where many mesoscale eddies occur is largely due to synoptic features such as extratropical cyclones, fronts, and atmospheric rivers, especially in winter (Catto & Pfahl, 2013; Konstali et al., 2024; Soster & Parfitt, 2022; Utsumi et al., 2017). Therefore, the interaction of mesoscale eddies and oceanic fronts or WBCs with the atmospheric synoptic features is important. Recent work has demonstrated that atmospheric fronts do indeed respond to underlying SST and its gradients (Parfitt et al., 2016) although it is dependent on the type of front—long lasting or more local (Reeder et al., 2021). Further, studies have shown that increased resolution significantly improves the representation of mesoscale storm dynamics, frontal sharpness, and latent heating processes, all of which are crucial for capturing realistic precipitation distributions (Bauer et al., 2015; Smirnov et al., 2015; Soster & Parfitt, 2022; Willison et al., 2013; Wu & Ma, 2025). In this study, we examine precipitation response to mesoscale SSTs using an approximately 25 km atmosphere-land model coupled to a nominal 10 km ocean-sea ice model, which has been shown to well capture extreme precipitation (Chang et al., 2025).

In climate models and reanalysis, a substantial portion of precipitation—particularly that arising from unresolved convective processes—is represented through sub-grid-scale parameterizations. These parameterizations include: (a) convective scheme (deep and shallow), (b) microphysical scheme, as well as (c) cloud macrophysics, radiation and planetary boundary layer (PBL) schemes (e.g. discussion in Bogenschutz et al., 2018). Only storm-resolving models at kilometer-scale resolutions (e.g., Caldwell et al., 2021; Gentile et al., 2025; Judt & Rios-Berrios, 2021; Stevens et al., 2019) can dispense of schemes like deep convection, as they start to permit or resolve the key deep-convective processes. Therefore, for the climate models and reanalysis in general use and discussed in this study, a reasonable representation of the precipitation response to SST relies heavily on the performance of the parameterization schemes, particularly (a) and (b) (but also dependent on schemes like PBL). A novel aspect of this study is to assess the performance of these schemes in representing local precipitation response to mesoscale SST variability in climate models depends on the choice of convective parameterization scheme. To the best of our knowledge, few studies have done such an analysis in models of fine enough resolution to mostly resolve the mesoscale SST features (but not fine enough to resolve convection). In this study, we explore the local precipitation response to SST variability in observations, reanalysis, and climate models of different resolutions, with a focus on the role of convective parameterization. Understanding this issue is important because it is pertinent to the question whether this class of high-resolution climate models is fully capable of representing the effect of mesoscale SST on the atmosphere and climate.

2. Materials and Methods

2.1. Data Sets

We use the high-resolution Optimum Interpolation (OI) SST (OISST) Version 2 (V2) data set from the National Oceanic and Atmospheric Administration (NOAA) for SST analysis (Reynolds et al., 2007). Specifically, we use

the monthly mean OISST with a spatial resolution of 0.25° from 1981 to 2022 as the observed SST data set to explore SST-precipitation relationships and as a benchmark for model comparisons.

For precipitation, we use the Integrated Multi-Satellite Retrievals for Global Precipitation Measurement (IMERG) product from the National Aeronautics and Space Administration (NASA) (Huffman et al., 2020). IMERG provides estimates at 30-min, daily and monthly intervals with a high spatial resolution of 0.1°. In this study, we use monthly IMERG Version 6 (IMERGv6) data from 2000 onwards. Prior studies demonstrate that it performs well in capturing global and regional precipitation patterns (Beck et al., 2017; Sun et al., 2018).

To analyze circulation anomalies associated with precipitation variability, we use ERA5, the fifth-generation atmospheric reanalysis from the European Centre for Medium-Range Weather Forecasts (ECMWF) (Hersbach et al., 2020). ERA5 provides global coverage at a horizontal resolution of 31 km (spectral TL639) with 137 vertical levels and employs a 4D-VAR ensemble data assimilation. It also incorporates an enhanced version of the Tiedtke (1989) convection parameterization scheme (see Table S1 in Supporting Information S1). For this study, we use ERA5 data on a 0.25° output grid, selecting variables including SST, vertical velocity, and precipitation. Our analysis focuses on the period from 2001 to 2016, when satellite data coverage was more extensive (Hersbach et al., 2020). ERA5 has been extensively validated and widely employed as a proxy for observational data sets in numerous previous studies, particularly in scenarios where direct observations are sparse or unavailable (Albergel et al., 2018; Hersbach et al., 2020; Tetzner et al., 2019). However, as discussed in Small et al. (2023), ERA5 tends to underestimate some boundary layer responses to SST, and Masunaga and Schneider (2022) revealed that ERA5 underestimated the wind response to SST by 20%–30% on average.

2.2. Low- and High-Resolution Community Earth System Model (CESM)

CESM1 (Hurrell et al., 2013) comprises the Community Atmosphere Model (CAM5) coupled to the Parallel Ocean Program (POP2) ocean, Community Land Model (CLM4) and CICE5 sea ice models. This study uses CESMv1.3 with a Spectral Element dynamical core CAM5 (Meehl et al., 2019). The standard low-resolution configuration (CESM-LR) uses a horizontal resolution of nominal 1° for all components, while the high-resolution configuration (CESM-HR) uses nominal 0.25° for CAM5 and CLM4 and 0.1° for POP2 and CICE4. Both CESM-LR and CESM-HR employ a deep convection parameterization scheme developed by Zhang and McFarlane (1995) and modified with the addition of convective momentum transports by Richter and Rasch (2008) and a modified dilute plume calculation (Raymond & Blyth, 1986, 1992) (see Table S1 in Supporting Information S1).

CESM-HR and CESM-LR had extensive equilibration periods with long (500 years) pre-industrial controls (PI-CTL), accompanied by a historical (1850–1920) run branched at year 250 of PI-CTL, and an ensemble of 10 historical (1920–2005) and future (2006–2100) climate simulations under Representative Concentration Pathway (RCP) 6.0 and 8.5 emission scenario, respectively (Chang et al., 2020). Here, the simulation output from a 3-member ensemble for 1950–2005 (Chang et al., 2023) with a monthly temporal resolution is used to address the objectives in this study.

2.3. High-Resolution Model Intercomparison Project (HighResMIP) Data

The HighResMIP protocol facilitated the use of high-resolution modelling by having short spin-up periods (30 years) followed by a 100-year control for year 1950 conditions, and a transient run for 1950 to 2050 (Haarsma et al., 2016; Roberts et al., 2019; Roberts, Camp, et al., 2020; Roberts, Jackson, et al., 2020) under Shared Socioeconomic Pathway 5-8.5 (SSP5-8.5) scenario.

The models analyzed in this paper are: CNRM-CM6-1-HR (Saint-Martin et al., 2021), EC-EARTH3P-HR (Haarsma et al., 2020), HadGEM3-GC31-HM (Roberts et al., 2019), and MPI-ESM1-2-XR (Gutjahr et al., 2019) with more details given in Table S1 of Supporting Information S1. All models have a 0.25° ocean grid except MPI with 0.4°, and all have a 0.5° atmosphere grid. Thus, the resolution of these models is coarser than that of CESM-HR, but higher than the standard CMIP6 models. These four models were selected because they represent some of the highest-resolution configurations available within HighResMIP, span a diversity of convective parameterization schemes, and provide complete data availability across all HighResMIP simulations analyzed in this study.

In addition to the coupled simulations, we also employ the HighResMIP HighresSST-present atmosphere–only experiments as a parallel control analysis, which use prescribed SST and sea-ice forcing. According to the HighResMIP protocol (Haarsma et al., 2016), these forced-atmosphere runs are driven by HadISST2.2.0.0 1/4° daily SST and sea-ice forcing data set, uniformly applied across all participating models.

3. Results

3.1. Regional Precipitation Related to Mesoscale SST Variability

To examine how regional precipitation response to mesoscale SST variability in ocean frontal regions behaves differently in high- and low-resolution climate simulations, we first applied a two-dimensional (2-D) boxcar filter with a cutoff wavelength of 5° × 5° to separate mesoscale variability from large-scale variability in both model and observational data sets, closely following Liu et al. (2018). With this filter applied, maps of SST variance clearly highlight the WBCs in both observations and CESM-HR simulations, whereas these high-variance regions are absent in CESM-LR (Figure S1 in Supporting Information S1), indicating CESM-HR's superiority in capturing mesoscale SST variability.

Figure 1 depicts point-wise correlation coefficients between concurrent high-pass filtered precipitation and SST anomalies. In WBCs with abundant eddies and meanders, precipitation and SST anomalies exhibit positive correlations (typically 0.3 to 0.5) in both observations and ERA5 (Figures 1a and 1h) with most correlations statistically significant at the 95% level (Figure S2 in Supporting Information S1). Some interesting regional differences are seen—in the satellite data (Figure 1a), the Agulhas Return Current/Southern Ocean has a clearer signal than the Gulf Stream. In related work (L. Laurindo, pers. Comm. 2024), when composited on ocean mesoscale eddies, precipitation tends to peak over the SST in the Agulhas/Southern Ocean, while in the Gulf Stream/North Atlantic, a spatial downwind lag of precipitation from SST of up to an eddy radius is observed—potentially explaining the weaker local correlations found over the Gulf Stream in satellite data. A similar picture to ERA5 and satellite data appears in CESM-HR (Figure 1b), whereas CESM-LR shows strong correlations only in the Tropics (Figure 1g).

We next analyze only points with strong precipitation-SST correlation (>0.4) in the Gulf Stream (GS, Figures 2a–2c) and Agulhas Current (AC, Figures S3a–S3c in Supporting Information S1), and separate the simulated precipitation into large-scale and parameterized convective components. CESM-LR results are omitted, as its regression slopes are near zero or not significant (Figure S2 in Supporting Information S1). The comparison in Figure 2a suggests that the response of precipitation to SST variability at mesoscale in CESM-HR closely resembles the observations, though slightly underestimated. Further analyses show that substantial correlations and regressions between precipitation and SST anomalies in the extratropics are primarily attributed to the parameterized convective component. For example, in the GS, CESM-HR attributes 0.193 mm day^{-1} $°C^{-1}$ to convective parameterization (Figure 2b), while only 0.004 mm day^{-1} $°C^{-1}$ comes from resolved large-scale precipitation (Figure 2c). In ERA5, large-scale precipitation plays a bigger role (0.075 mm day^{-1} $°C^{-1}$, Figure 2c), but convective parameterization remains dominant (0.149 mm day^{-1} $°C^{-1}$, Figures 2a and 2b). Moreover, it is worth noting that although the resolved large-scale precipitation response shows a larger bias relative to ERA5 (Figure 2c), it plays only a minor role in the mesoscale SST–precipitation relationship. The pronounced reliance on convective parameterization, particularly in CESM-HR, highlights the scheme's influence on this coupling and warrants further study. The major contribution from convective parameterization component to total precipitation in CESM-HR and in ERA5 is also seen in the AC region, although the slopes in total precipitation are both weaker than the observation (Figures S3a–S3c in Supporting Information S1). Hence, the convective parameterization in ERA5 and CESM-HR provides a reasonable fit to total observed precipitation in IMERG, albeit with some underestimation. Resolved large-scale precipitation plays a secondary role, especially in CESM-HR, where it is negligible. This suggests that the dominant convective parameterization is working well in these cases, essentially by "making up" for the lack of resolved precipitation response.

To further explore the role of resolution and convective parameterization, we analyzed the available HighResMIP simulations. These simulations generally replicate the observed significant mesoscale SST-precipitation relationships in extratropical, eddy-rich ocean frontal regions (Figures 1c–1f). However, the EC-EARTH3P-HR model (Figure 1d) greatly overestimates the correlation compared to satellite data and ERA5 (Figures 1a and 1h), while MPI-ESM1-2-XR has unusual negative values in low latitudes (Figure 1f). It is worth noting that EC-EARTH3P-HR employs a similar convection scheme to ERA5 (Table S1 in Supporting Information S1) but

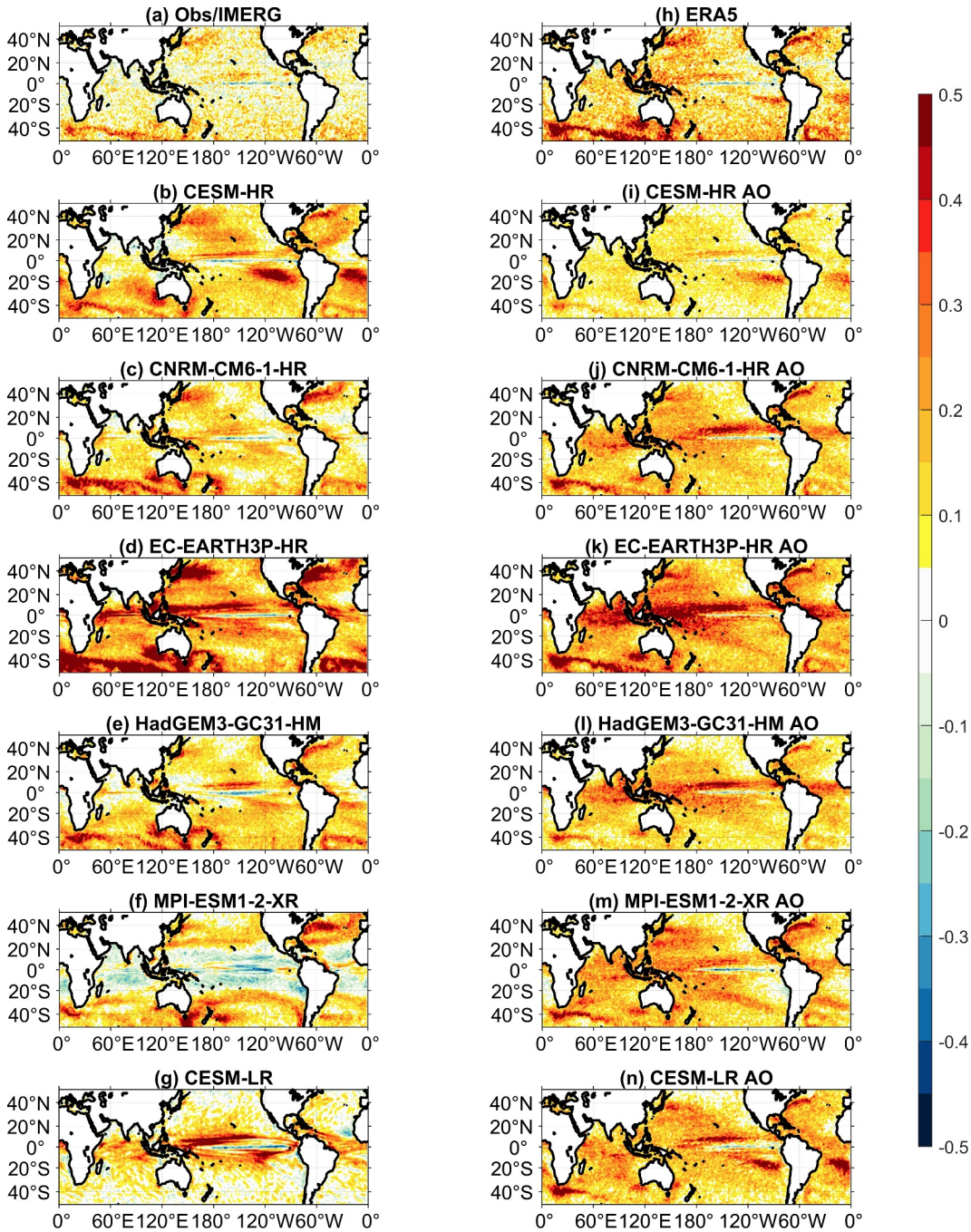

Figure 1. Simultaneous correlation coefficients between spatially highpass-filtered monthly mean SST and precipitation anomalies. (a) Observations and (h) ERA5 reanalysis data for the period 2001–2016. (b–n) A single ensemble member of various climate models for the period 1950–2005: (b, i) CESM-HR, (g, n) CESM-LR, and (c–f, j–m) HighResMIP models, including (c, j) CNRM-CM6-1-HR, (d, k) EC-EARTH3P-HR, (e, l) HadGEM3-GC31-HM, and (f, m) MPI-ESM1-2-XR. Panels (b–g) show results from coupled simulations, and panels (i–n) show results from atmosphere–only (AO) simulations.

has coarser atmosphere grid spacing (0.5° vs. 0.31° in ERA5) and no data assimilation. These models have some differences in mesoscale SST variance (Figure S4 in Supporting Information S1) and background SST. To reduce uncertainty induced by the different SST, a parallel analysis of HighResMIP atmosphere-land-only simulations (similar to Atmosphere Model Intercomparison Project protocol, and referred to as AMIP here) is presented in Figures 1j–1m. Notably, in terms of correlation between SST and precipitation, the AMIP simulations exhibit

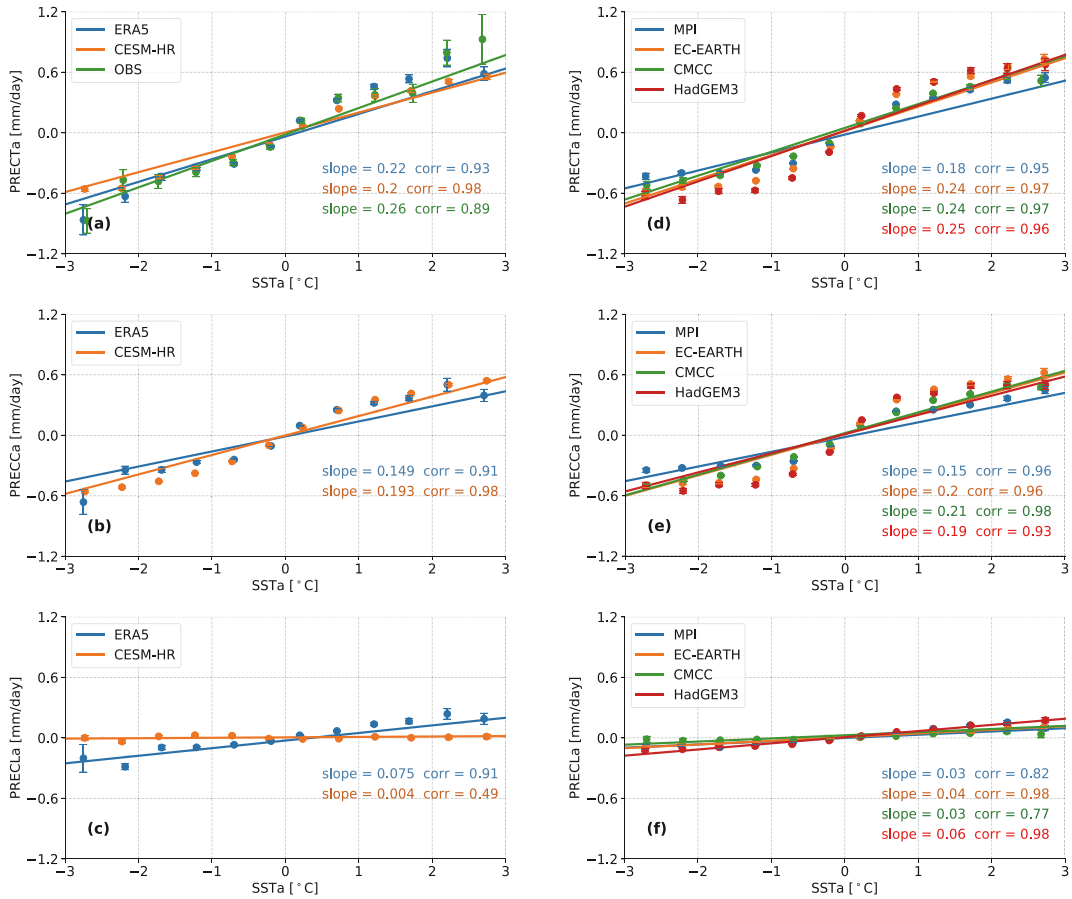

Figure 2. Scatterplots of mesoscale monthly SST and precipitation anomalies in GS (45–70°W, 36–42°N). (a–c) Show results from observations, ERA5 reanalysis, and CESM-HR, while (d–f) display results from HighResMIP models. All points where the significant correlation is larger than 0.4 are chosen. (a, d) Scatterplots of mesoscale SST and total precipitation (PRECT) anomalies, (b, e) scatterplots of mesoscale SST and convective precipitation (PRECC) anomalies, and (c, f) scatterplots of mesoscale SST and large-scale precipitation (PRECL) anomalies.

greater consistency across models than their coupled counterparts, suggesting that background SST and SST variability in the coupled runs causes a large spread of correlation results. For example, the EC-EARTH3P-HR AMIP case now has more comparable mesoscale SST-precipitation correlation in WBCs (Figure 1k) and MPI-ESM1-2-XR AMIP no longer exhibits the extensive region of negative correlations (Figure 1m). Meanwhile, for CESM, the AMIP simulation gives correlations more similar to observed values than the coupled case (Figure 1i), while the low-resolution atmosphere equivalent gives a stronger response (Figure 1n). The latter result relates to a higher proportion of parameterized convective precipitation at low resolution compared to high-resolution (Chang et al., 2020) and possibly also due to more atmospheric variability (unrelated to SST) in high-resolution adding noise to the system.

As with CESM and ERA5, separating precipitation into parameterized convective (Figure 2e) and large-scale precipitation (Figure 2f) reveals that although the total precipitation responses vary across the models, the relative contribution from parameterized convective precipitation remains high and consistent, ranging from 74% to 92% (Figures 2d–2f). For both the GS and AC, MPI-ESM1-2-XR exhibits small regression values compared to other models and observations (Figure 2, Figure S3 in Supporting Information S1), while EC-EARTH3P-HR has higher regression values than ERA5 in the AC region (MPI-ESM1-2-XR, EC-EARTH3P-HR and ERA5 all use a Tiedke convection scheme but with varying updates and enhancements). Meanwhile, the HadGEM and CNRM high-resolution models exhibit similar characteristics to CESM-HR and ERA5 despite having coarser atmosphere grids (0.5°) and different convection schemes.

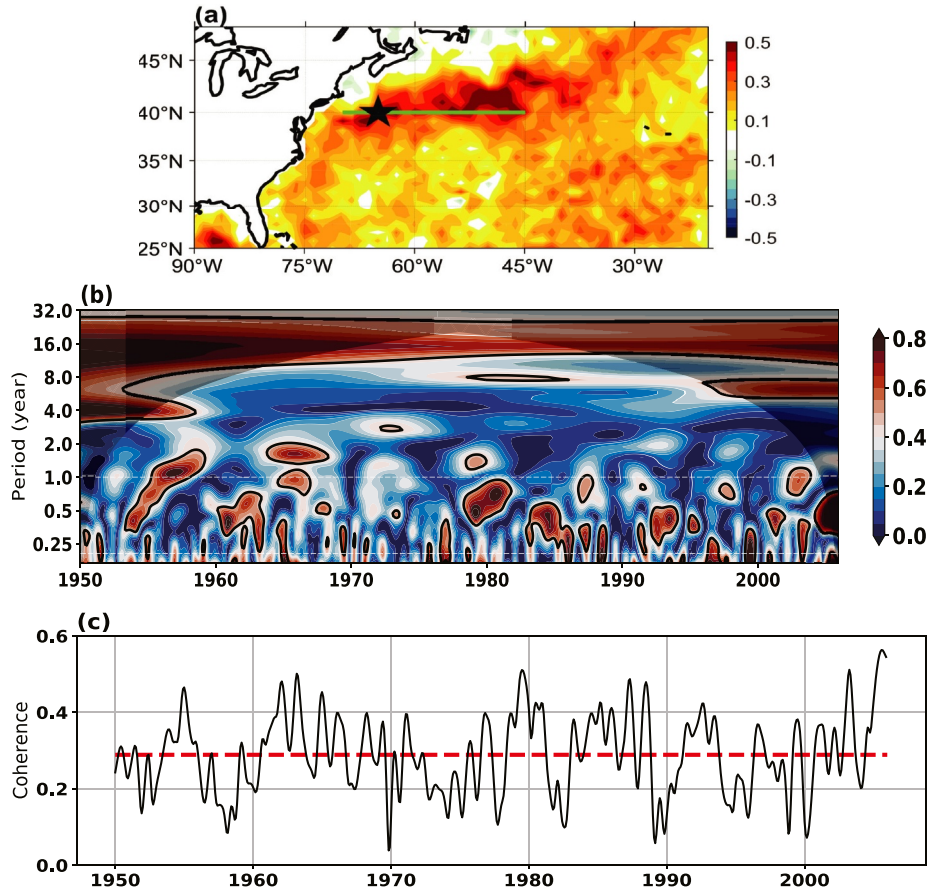

Figure 3. (a) Simultaneous pointwise correlation coefficient between monthly mesoscale SST and precipitation anomalies from CESM-HR in the GS region; (b) wavelet coherence between monthly mesoscale SST and precipitation anomalies at an example point (40°N, 65°W) (star in Figure 3a); (c) averaged coherence within temporal window between 2 and 12 months (black solid line) and criteria values (mean plus one standard deviation, red dashed line).

3.2. Extended Mid-Troposphere Response

The analysis conducted thus far relies on linear correlations and regressions between precipitation and SST anomalies, and the next step is to determine if the precipitation is primarily generated by MABL processes or if there are deeper convective responses linked to vertical circulation changes that extend into the free troposphere above the MABL. Understanding the vertical scale of convection is important because it determines the efficiency with which convective heating projects onto Rossby wave sources, influencing wave generation, propagation, and atmospheric teleconnections.

To answer this question, we employed a wavelet coherence analysis in a region of high mesoscale eddy variability, a section along 40°N in the GS, to identify events of strong air-sea coherence (Figure 3). Figure 3b illustrates high coherences of precipitation and SST predominantly occur within a temporal scale ranging from 2 to 12 months, for an example point at 40°N, 65°W. Next, the significant coherence within this specific temporal window is averaged (Figure 3c) and events whose coherence exceeds one standard deviation above the mean value are identified as strong coupling events. Composites are made by averaging local atmospheric responses over the time periods corresponding to these strong coupling events, which account for approximately 15%–17% of the total analysis period. The same approach is applied to CESM-LR and ERA5. The composite analysis results have been compared with the approach of using all positive high-pass filtered SST anomalies in the study region which gave similar results (not shown).

Figure 4 shows the composite of highpass-filtered vertical velocities over the GS for warm SST anomalies (Here we use ω to refer to negated vertical pressure velocities, so that positive ω denotes ascent). Local ascending

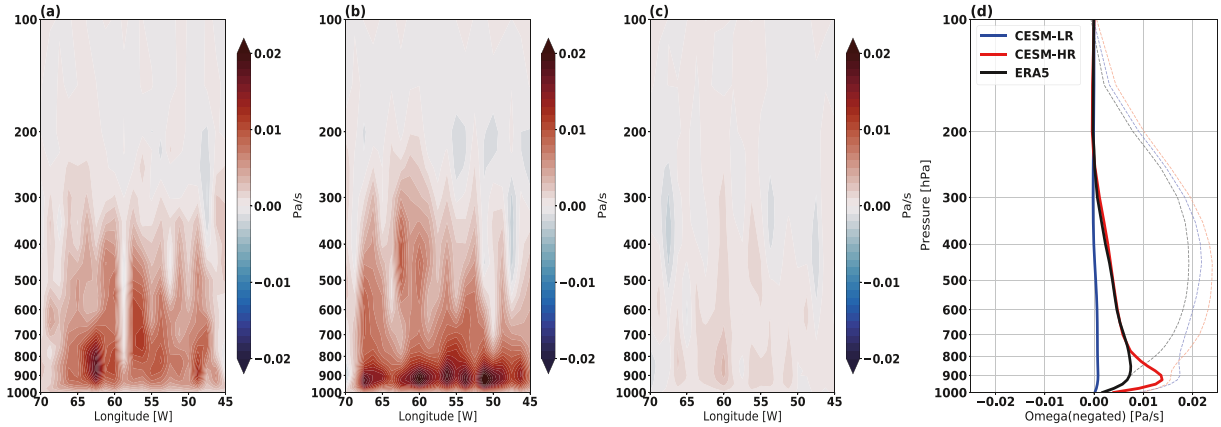

Figure 4. Composite of mean mesoscale omega (negated) anomaly (unit: Pas^{-1}) in targeted GS region along 40°N (green line in Figure 3a) for (a) ERA5, (b) CESM-HR, and (c) CESM-LR. (d) Composite of mean mesoscale omega (negated) anomaly (unit: Pas^{-1}, solid lines) in targeted GS region (40°N, 70–45°W) for ERA (black), CESM-HR (red), and -LR (blue). Climatology omega (negated) values (unit: Pas^{-1}) are shown in dashed lines.

motions with maximum values near the top of the MABL are seen in both CESM-HR and ERA5. In comparison to climatological ω, which peaks near 500 hPa with values of approximately 0.02 Pas^{-1}, composite ω anomalies reveal a smaller maximum value at a lower level, around 900 to 850 hPa (Figure 4d). For ERA5, the maximum value of composite ω anomalies is around 0.007 Pas^{-1}, whereas for CESM-HR it is approximately twice as large, around 0.013 Pas^{-1}, so that vertical velocity anomalies induced by mesoscale SST anomalies are roughly 30%–50% of climatological values (Figure 4d). Even though the anomalies exhibit shallower vertical extent than the climatological profile, at the mid troposphere around 500 hPa, the anomalous ω retains a value of approximately 0.003 Pas^{-1}, which is about 10%–15% of the maximum climatological value.

In contrast, such a vertical velocity response to mesoscale SST anomalies is conspicuously absent in CESM-LR (Figure 4d, blue), consistent with the lack of mesoscale SST variability, which hampers the model's ability to simulate small-scale precipitation and associated circulation response over the GS. Similar results are found in the KE, as depicted in Figure S5 of Supporting Information S1.

4. Conclusion and Discussion

Taken together, analyses of satellite data, CESM-HR, HighResMIP simulations and ERA5 consistently reveal an atmospheric response to mesoscale SST variability that extends beyond the MABL. However, the magnitude of the response differs between data sets. In reanalysis and climate models, the response is primarily driven by parameterized convective precipitation, making it highly sensitive to that parameterization scheme. In addition, comparative analysis of fully coupled models and atmosphere-only simulations revealed a dependence of the response on model SST - both on the background SST, influenced by biases in coupled models to which convection is highly sensitive, as well as on the SST variability, which can influence whether precipitation responses rise above noise. This underscores the need to determine whether this class of high-resolution models with atmospheric resolution of 25–50 km captures the response for the right reasons. Such uncertainty may hinder their ability to accurately simulate the remote impacts of mesoscale SST forcing, as the vertical profile of the diabatic heating associated with mesoscale SST forcing is critical for determining the remote atmospheric response. To further address these issues, future studies should employ storm-resolving model simulations that explicitly resolve deep convective processes, rather than relying on convective parameterization schemes.

The processes underlying the precipitation response to SST are not discussed in this paper, but analysis of high-frequency data (daily in this case) provides some insight, specifically on the influence of extremes. The correlation of monthly precipitation and SST was repeated, but now using particular percentiles of precipitation based on the daily data within each month, instead of monthly mean. For strong events (90th percentile here) the correlation was found to be weaker than that for the mean, in ERA5 and CESM-HR (compare Supp. Figure S6a in Supporting Information S1 with Figure 1h, and Figure S6c in Supporting Information S1 with Figure 1b). Meanwhile, weak events (tenth percentile) showed correlations similar to the monthly mean, or slightly stronger

(see Supp. Figures S6b and S6d in Supporting Information S1). The results suggest that mesoscale SST fluctuations influence the overall climate background rather than strong and extreme weather events, although further work is needed on this topic (e.g. on determining whether extreme event responses overlie the SST, or not).

Conflict of Interest

The authors declare no conflicts of interest relevant to this study.

Data Availability Statement

Observational SST data set-OISST data set, the high-resolution Optimum Interpolation (OI) SST (OISST) Version 2 (V2), can be obtained from https://www.ncei.noaa.gov/products/optimum-interpolation-sst. The Integrated Multi-Satellite Retrievals for Global Precipitation Measurement (IMERG) product (Huffman et al., 2020), can be obtained from https://gpm.nasa.gov/resources/documents/imerg-v06-release-notes. ERA5 can be obtained from https://doi.org/10.24381/cds.f17050d7 (Copernicus Climate Change Service, 2023). Low- and High-resolution CESM is available from https://rda.ucar.edu/datasets/d651007/. High-resolution Model Intercomparison Project data were obtained from https://esgf-node.ipsl.upmc.fr/projects/cmip6-ipsl/ (Castruccio, 2024). The code for the analysis and to reproduce the results can be found at https://doi.org/10.18738/T8/RT7J5C, Texas Data Repository (Wang, 2024).

Acknowledgments
This study is based in part on X. Wang's doctoral dissertation research at Texas A&M University under the supervision of P. Chang. We acknowledge support from NSF Grants AGS-2231237 and AGS-2332469, as well as the Department of Commerce through NOAA OAR's Climate Variability and Predictability Program (NA24OARX431G0047). We also acknowledge the CESM project and the computational resources provided by the Texas Advanced Computing Center (TACC; http://www.tacc.utexas.edu) at the University of Texas at Austin, and Derecho (https://doi.org/10.5065/qx9a-pg09) at the Computational and Information Systems Laboratory (CISL) of the NSF National Center for Atmospheric Research (NCAR). NSF NCAR is a major facility sponsored by the U.S. NSF under Cooperative Agreement 1852977.

References

Albergel, C., Dutra, E., Munier, S., Calvet, J.-C., Munoz-Sabater, J., de Rosnay, P., & Balsamo, G. (2018). ERA-5 and ERA-Interim driven ISBA land surface model simulations: Which one performs better? *Hydrology and Earth System Sciences*, *22*(6), 3515–3532. https://doi.org/10.5194/hess-22-3515-2018

Alexander, M. A., Bladé, I., Newman, M., Lanzante, J. R., Lau, N.-C., & Scott, J. D. (2002). The atmospheric bridge: The influence of ENSO teleconnections on air–sea interaction over the global oceans. *Journal of Climate*, *15*(16), 2205–2231. https://doi.org/10.1175/1520-0442(2002)015<2205:tabtio>2.0.co;2

Bauer, P., Thorpe, A., & Brunet, G. (2015). The quiet revolution of numerical weather prediction. *Nature*, *525*(7567), 47–55. https://doi.org/10.1038/nature14956

Beck, H. E., Vergopolan, N., Pan, M., Levizzani, V., Van Dijk, A. I., Weedon, G. P., et al. (2017). Global-scale evaluation of 22 precipitation datasets using gauge observations and hydrological modeling. *Hydrology and Earth System Sciences*, *21*(12), 6201–6217. https://doi.org/10.5194/hess-21-6201-2017

Bishop, S. P., Small, R. J., Bryan, F. O., & Tomas, R. A. (2017). Scale dependence of midlatitude air–sea interaction. *Journal of Climate*, *30*(20), 8207–8221. https://doi.org/10.1175/jcli-d-17-0159.1

Bogenschutz, P. A., Gettelman, A., Hannay, C., Larson, V. E., Neale, R. B., Craig, C., & Chen, C.-C. (2018). The path to CAM6: Coupled simulations with CAM5. 4 and CAM5. 5. *Geoscientific Model Development*, *11*(1), 235–255. https://doi.org/10.5194/gmd-11-235-2018

Caldwell, P. M., Terai, C. R., Hillman, B., Keen, N. D., Bogenschutz, P., Lin, W., et al. (2021). Convection-permitting simulations with the E3SM global atmosphere model. *Journal of Advances in Modeling Earth Systems*, *13*(11), e2021MS002544. https://doi.org/10.1029/2021ms002544

Castruccio, F., Chang, P., Danabasoglu, G., Fu, D., Rosenbloom, N., Zhang, Q., et al. (2024). MESACLIP: A 10-member ensemble of CESM HR historical (1920–2005) simulations [Dataset]. *NSF National Center for Atmospheric Research*. https://doi.org/10.5065/7N1X-K278

Catto, J. L., & Pfahl, S. (2013). The importance of fronts for extreme precipitation. *Journal of Geophysical Research: Atmospheres*, *118*(19), 791–710. https://doi.org/10.1002/jgrd.50852

Chang, P., Fu, D., Liu, X., Castruccio, F. S., Prein, A. F., Danabasoglu, G., et al. (2025). Future extreme precipitation amplified by intensified mesoscale moisture convergence. *Nature Geoscience*, *19*, 1–9. https://doi.org/10.1038/s41561-025-01859-1

Chang, P., Xu, G., Kurian, J., Small, R. J., Danabasoglu, G., Yeager, S., et al. (2023). Uncertain future of sustainable fisheries environment in eastern boundary upwelling zones under climate change. *Communications Earth and Environment*, *4*(1), 19. https://doi.org/10.1038/s43247-023-00681-0

Chang, P., Zhang, S., Danabasoglu, G., Yeager, S. G., Fu, H., Wang, H., et al. (2020). An unprecedented set of high-resolution earth system simulations for understanding multiscale interactions in climate variability and change. *Journal of Advances in Modeling Earth Systems*, *12*(12), e2020MS002298. https://doi.org/10.1029/2020ms002298

Chelton, D. B., & Xie, S.-P. (2010). Coupled ocean-atmosphere interaction at oceanic mesoscales. *Oceanography*, *23*(4), 52–69. https://doi.org/10.5670/oceanog.2010.05

Copernicus Climate Change Service. (2023). ERA5 monthly averaged data on single levels from 1940 to present [Dataset]. *Copernicus Climate Change Service (C3S) Climate Data Store (CDS)*. https://doi.org/10.24381/cds.f17050d7

Cronin, M., & Watts, D. R. (1996). Eddy–mean flow interaction in the Gulf Stream at 68 W. Part I: Eddy energetics. *Journal of Physical Oceanography*, *26*(10), 2107–2131. https://doi.org/10.1175/1520-0485(1996)026<2107:efiitg>2.0.co;2

Foussard, A., Lapeyre, G., & Plougonven, R. (2019). Storm track response to oceanic eddies in idealized atmospheric simulations. *Journal of Climate*, *32*(2), 445–463. https://doi.org/10.1175/jcli-d-18-0415.1

Frenger, I., Gruber, N., Knutti, R., & Münnich, M. (2013). Imprint of Southern Ocean eddies on winds, clouds and rainfall. *Nature Geoscience*, *6*(8), 608–612. https://doi.org/10.1038/ngeo1863

Gentile, E. S., Harris, L., Zhao, M., Hodges, K., Tan, Z., Cheng, K. Y., & Zhou, L. (2025). Response of extreme north Atlantic midlatitude cyclones to a warmer climate in the GFDL X-SHiELD kilometer-scale global storm-resolving model. *Geophysical Research Letters*, *52*(2), e2024GL112570. https://doi.org/10.1029/2024gl112570

Gill, A. E., & Rasmusson, E. M. (1983). The 1982–83 climate anomaly in the equatorial Pacific. *Nature*, *306*(5940), 229–234. https://doi.org/10.1038/306229a0

Gutjahr, O., Putrasahan, D., Lohmann, K., Jungclaus, J. H., von Storch, J.-S., Brüggemann, N., et al. (2019). Max Planck institute Earth system model (MPI-ESM1. 2) for the High-Resolution Model Intercomparison Project (HighResMIP). *Geoscientific Model Development*, *12*(7), 3241–3281. https://doi.org/10.5194/gmd-12-3241-2019

Haarsma, R. J., Acosta, M., Bakhshi, R., Bretonnière, P.-A. B., Caron, L.-P., Castrillo, M., et al. (2020). HighResMIP versions of EC-Earth: Ec-earth3p and EC-Earth3P-HR. Description, model performance, data handling and validation. *Geoscientific Model Development Discussions*, *2020*, 1–37.

Haarsma, R. J., Roberts, M. J., Vidale, P. L., Senior, C. A., Bellucci, A., Bao, Q., et al. (2016). High resolution model intercomparison project (HighResMIP v1. 0) for CMIP6. *Geoscientific Model Development*, *9*(11), 4185–4208. https://doi.org/10.5194/gmd-9-4185-2016

Hersbach, H., Bell, B., Berrisford, P., Hirahara, S., Horányi, A., Muñoz-Sabater, J., et al. (2020). The ERA5 global reanalysis. *Quarterly Journal of the Royal Meteorological Society*, *146*(730), 1999–2049. https://doi.org/10.1002/qj.3803

Horel, J. D., & Wallace, J. M. (1981). Planetary-scale atmospheric phenomena associated with the Southern Oscillation. *Monthly Weather Review*, *109*(4), 813–829. https://doi.org/10.1175/1520-0493(1981)109<0813:psapaw>2.0.co;2

Hoskins, B. J., & Karoly, D. J. (1981). The steady linear response of a spherical atmosphere to thermal and orographic forcing. *Journal of the Atmospheric Sciences*, *38*(6), 1179–1196. https://doi.org/10.1175/1520-0469(1981)038<1179:tslroa>2.0.co;2

Huffman, G. J., Bolvin, D. T., Braithwaite, D.,Hsu, K.-L., Joyce, R. J., Kidd, C., et al. (2020). Integrated multi-satellite retrievals for the Global Precipitation Measurement (GPM) Mission (IMERG). In *Satellite precipitation measurement* (Vol. 1, pp. 343–353). Springer.

Hurrell, J. W., Holland, M. M., Gent, P. R., Ghan, S., Kay, J. E., Kushner, P. J., et al. (2013). The community earth system model: A framework for collaborative research. *Bulletin of the American Meteorological Society*, *94*(9), 1339–1360. https://doi.org/10.1175/bams-d-12-00121.1

Judt, F., & Rios-Berrios, R. (2021). Resolved convection improves the representation of equatorial waves and tropical rainfall variability in a global nonhydrostatic model. *Geophysical Research Letters*, *48*(14), e2021GL093265. https://doi.org/10.1029/2021gl093265

Kelly, K. A., Small, R. J., Samelson, R., Qiu, B., Joyce, T. M., Kwon, Y.-O., & Cronin, M. F. (2010). Western boundary currents and frontal air–sea interaction: Gulf Stream and Kuroshio extension. *Journal of Climate*, *23*(21), 5644–5667. https://doi.org/10.1175/2010jcli3346.1

Konstali, K., Spensberger, C., Spengler, T., & Sorteberg, A. (2024). Global attribution of precipitation to weather features. *Journal of Climate*, *37*(4), 1181–1196. https://doi.org/10.1175/jcli-d-23-0293.1

Kuwano-Yoshida, A., & Minobe, S. (2017). Storm-track response to SST fronts in the northwestern Pacific region in an AGCM. *Journal of Climate*, *30*(3), 1081–1102. https://doi.org/10.1175/jcli-d-16-0331.1

Kwon, B., Bénech, B., Lambert, D., Durand, P., Druilhet, A., Giordani, H., & Planton, S. (1998). Structure of the marine atmospheric boundary layer over an oceanic thermal front: SEMAPHORE experiment. *Journal of Geophysical Research*, *103*(C11), 25159–25180. https://doi.org/10.1029/98jc02207

Larson, J. G., Thompson, D. W. J., & Hurrell, J. W. (2024). Signature of the western boundary currents in local climate variability. *Nature*, *634*(8035), 862–867. https://doi.org/10.1038/s41586-024-08019-2

Lindzen, R. S., & Nigam, S. (1987). On the role of sea surface temperature gradients in forcing low-level winds and convergence in the tropics. *Journal of the Atmospheric Sciences*, *44*(17), 2418–2436. https://doi.org/10.1175/1520-0469(1987)044<2418:otross>2.0.co;2

Liu, X., Chang, P., Kurian, J., Saravanan, R., & Lin, X. (2018). Satellite-observed precipitation response to ocean mesoscale eddies. *Journal of Climate*, *31*(17), 6879–6895. https://doi.org/10.1175/jcli-d-17-0668.1

Liu, X., Ma, X., Chang, P., Jia, Y., Fu, D., Xu, G., et al. (2021). Ocean fronts and eddies force atmospheric rivers and heavy precipitation in western North America. *Nature Communications*, *12*(1), 1268. https://doi.org/10.1038/s41467-021-21504-w

Ma, X., Chang, P., Saravanan, R., Montuoro, R., Hsieh, J.-S., Wu, D., et al. (2015). Distant influence of Kuroshio eddies on North Pacific weather patterns? *Scientific Reports*, *5*(1), 17785. https://doi.org/10.1038/srep17785

Ma, X., Chang, P., Saravanan, R., Montuoro, R., Nakamura, H., Wu, D., et al. (2017). Importance of resolving Kuroshio front and eddy influence in simulating the North Pacific storm track. *Journal of Climate*, *30*(5), 1861–1880. https://doi.org/10.1175/jcli-d-16-0154.1

Marshall, J., Ferrari, R., Forget, G., Maze, G., Andersson, A., Bates, N., et al. (2009). The CLIMODE field campaign: Observing the cycle of convection and restratification over the Gulf Stream. *Bulletin of the American Meteorological Society*, *90*(9), 1337–1350.

Masunaga, R., & Schneider, N. (2022). Surface wind responses to Mesoscale Sea surface temperature over western boundary current regions assessed by spectral transfer functions. *Journal of the Atmospheric Sciences*, *79*(6), 1549–1573. https://doi.org/10.1175/jas-d-21-0125.1

Matsuno, T. (1966). Quasi-geostrophic motions in the equatorial area. *Journal of the Meteorological Society of Japan. Series II*, *44*(1), 25–43. https://doi.org/10.2151/jmsj1965.44.1_25

Meehl, G. A., Yang, D., Arblaster, J. M., Bates, S. C., Rosenbloom, N., Neale, R., et al. (2019). Effects of model resolution, physics, and coupling on Southern Hemisphere storm tracks in CESM1. 3. *Geophysical Research Letters*, *46*(21), 12408–12416. https://doi.org/10.1029/2019gl084057

Minobe, S., Kuwano-Yoshida, A., Komori, N., Xie, S.-P., & Small, R. J. (2008). Influence of the Gulf Stream on the troposphere. *Nature*, *452*(7184), 206–209. https://doi.org/10.1038/nature06690

Nakamura, H., Sampe, T., Tanimoto, Y., & Shimpo, A. (2004). Observed associations among storm tracks, jet streams and midlatitude oceanic fronts. *Earth's Climate: The Ocean–Atmosphere Interaction, Geophysical Monograph*, *147*, 329–345.

O'Neill, L. W., Chelton, D. B., Esbensen, S. K., & Wentz, F. J. (2005). High-resolution satellite measurements of the atmospheric boundary layer response to SST variations along the Agulhas Return Current. *Journal of Climate*, *18*(14), 2706–2723.

Parfitt, R., Czaja, A., Minobe, S., & Kuwano-Yoshida, A. (2016). The atmospheric frontal response to SST perturbations in the Gulf Stream region. *Geophysical Research Letters*, *43*(5), 2299–2306. https://doi.org/10.1002/2016gl067723

Raymond, D. J., & Blyth, A. M. (1986). A stochastic mixing model for nonprecipitating cumulus clouds. *Journal of the Atmospheric Sciences*, *43*(22), 2708–2718. https://doi.org/10.1175/1520-0469(1986)043<2708:asmmfn>2.0.co;2

Raymond, D. J., & Blyth, A. M. (1992). Extension of the stochastic mixing model to cumulonimbus clouds. *Journal of the Atmospheric Sciences*, *49*(21), 1968–1983. https://doi.org/10.1175/1520-0469(1992)049<1968:eotsmm>2.0.co;2

Reeder, M. J., Spengler, T., & Spensberger, C. (2021). The effect of sea surface temperature fronts on atmospheric frontogenesis. *Journal of the Atmospheric Sciences*, *78*(6), 1753–1771. https://doi.org/10.1175/jas-d-20-0118.1

Reynolds, R. W., Smith, T. M., Liu, C., Chelton, D. B., Casey, K. S., & Schlax, M. G. (2007). Daily high-resolution-blended analyses for sea surface temperature. *Journal of Climate*, *20*(22), 5473–5496. https://doi.org/10.1175/2007jcli1824.1

Richter, J. H., & Rasch, P. J. (2008). Effects of convective momentum transport on the atmospheric circulation in the Community Atmosphere Model, version 3. *Journal of Climate*, *21*(7), 1487–1499. https://doi.org/10.1175/2007jcli1789.1

Roberts, M. J., Baker, A., Blockley, E. W., Calvert, D., Coward, A., Hewitt, H. T., et al. (2019). Description of the resolution hierarchy of the global coupled HadGEM3-GC3. 1 model as used in CMIP6 HighResMIP experiments. *Geoscientific Model Development*, *12*(12), 4999–5028. https://doi.org/10.5194/gmd-12-4999-2019

Roberts, M. J., Camp, J., Seddon, J., Vidale, P. L., Hodges, K., Vannière, B., et al. (2020). Projected future changes in tropical cyclones using the CMIP6 HighResMIP multimodel ensemble. *Geophysical Research Letters*, *47*(14), e2020GL088662. https://doi.org/10.1029/2020gl088662

Roberts, M. J., Jackson, L. C., Roberts, C. D., Meccia, V., Docquier, D., Koenigk, T., et al. (2020). Sensitivity of the Atlantic meridional overturning circulation to model resolution in CMIP6 HighResMIP simulations and implications for future changes. *Journal of Advances in Modeling Earth Systems*, *12*(8), e2019MS002014. https://doi.org/10.1029/2019ms002014

Saint-Martin, D., Geoffroy, O., Voldoire, A., Cattiaux, J., Brient, F., Chauvin, F., et al. (2021). Tracking changes in climate sensitivity in CNRM climate models. *Journal of Advances in Modeling Earth Systems*, *13*(6), e2020MS002190. https://doi.org/10.1029/2020ms002190

Schneider, N. (2020). Scale and Rossby number dependence of observed wind responses to ocean-mesoscale sea surface temperatures. *Journal of the Atmospheric Sciences*, *77*(9), 3171–3192. https://doi.org/10.1175/jas-d-20-0154.1

Seager, R., Naik, N., & Vecchi, G. A. (2010). Thermodynamic and dynamic mechanisms for large-scale changes in the hydrological cycle in response to global warming. *Journal of Climate*, *23*(17), 4651–4668. https://doi.org/10.1175/2010jcli3655.1

Seo, H., O'Neill, L. W., Bourassa, M. A., Czaja, A., Drushka, K., Edson, J. B., et al. (2023). Ocean mesoscale and frontal-scale ocean–atmosphere interactions and influence on large-scale climate: A review. *Journal of Climate*, *36*(7), 1981–2013. https://doi.org/10.1175/jcli-d-21-0982.1

Small, R. J., deSzoeke, S. P., Xie, S., O'neill, L., Seo, H., Song, Q., et al. (2008). Air–sea interaction over ocean fronts and eddies. *Dynamics of Atmospheres and Oceans*, *45*(3–4), 274–319. https://doi.org/10.1016/j.dynatmoce.2008.01.001

Small, R. J., Rousseau, V., Parfitt, R., Laurindo, L., O'Neill, L., Masunaga, R., et al. (2023). Near-surface wind convergence over the Gulf Stream —The role of SST revisited. *Journal of Climate*, *36*(16), 5527–5548. https://doi.org/10.1175/jcli-d-22-0441.1

Small, R. J., Tomas, R. A., & Bryan, F. O. (2014). Storm track response to ocean fronts in a global high-resolution climate model. *Climate Dynamics*, *43*(3–4), 805–828. https://doi.org/10.1007/s00382-013-1980-9

Smirnov, D., Newman, M., Alexander, M. A., Kwon, Y.-O., & Frankignoul, C. (2015). Investigating the local atmospheric response to a realistic shift in the Oyashio sea surface temperature front. *Journal of Climate*, *28*(3), 1126–1147. https://doi.org/10.1175/jcli-d-14-00285.1

Soster, F., & Parfitt, R. (2022). On objective identification of atmospheric fronts and frontal precipitation in reanalysis datasets. *Journal of Climate*, *35*(14), 4513–4534. https://doi.org/10.1175/jcli-d-21-0596.1

Stevens, B., Satoh, M., Auger, L., Biercamp, J., Bretherton, C. S., Chen, X., et al. (2019). DYAMOND: The DYnamics of the Atmospheric general circulation modeled on Non-hydrostatic Domains. *Progress in Earth and Planetary Science*, *6*(1), 1–17. https://doi.org/10.1186/s40645-019-0304-z

Sun, Q., Miao, C., Duan, Q., Ashouri, H., Sorooshian, S., & Hsu, K. L. (2018). A review of global precipitation data sets: Data sources, estimation, and intercomparisons. *Reviews of Geophysics*, *56*(1), 79–107. https://doi.org/10.1002/2017rg000574

Taguchi, B., Nakamura, H., Nonaka, M., & Xie, S.-P. (2009). Influences of the Kuroshio/Oyashio Extensions on air–sea heat exchanges and storm-track activity as revealed in regional atmospheric model simulations for the 2003/04 cold season. *Journal of Climate*, *22*(24), 6536–6560. https://doi.org/10.1175/2009jcli2910.1

Tetzner, D., Thomas, E., & Allen, C. (2019). A validation of ERA5 reanalysis data in the Southern Antarctic peninsula—Ellsworth land region, and its implications for ice core studies. *Geosciences*, *9*(7), 289. https://doi.org/10.3390/geosciences9070289

Tiedtke, M. (1989). A comprehensive mass flux scheme for cumulus parameterization in large-scale models. *Monthly Weather Review*, *117*(8), 1779–1800. https://doi.org/10.1175/1520-0493(1989)117<1779:acmfsf>2.0.co;2

Utsumi, N., Kim, H., Kanae, S., & Oki, T. (2017). Relative contributions of weather systems to mean and extreme global precipitation. *Journal of Geophysical Research: Atmospheres*, *122*(1), 152–167. https://doi.org/10.1002/2016jd025222

Wang, X. (2024). *Mesoscale publication codes*. Texas Data Repository, (Vol. V1).

Willison, J., Robinson, W. A., & Lackmann, G. M. (2013). The importance of resolving mesoscale latent heating in the North Atlantic storm track. *Journal of the Atmospheric Sciences*, *70*(7), 2234–2250. https://doi.org/10.1175/jas-d-12-0226.1

Woollings, T., Hannachi, A., & Hoskins, B. (2010). Variability of the North Atlantic eddy-driven jet stream. *Quarterly Journal of the Royal Meteorological Society*, *136*(649), 856–868. https://doi.org/10.1002/qj.625

Wu, R., Kirtman, B. P., & Pegion, K. (2006). Local air–sea relationship in observations and model simulations. *Journal of Climate*, *19*(19), 4914–4932. https://doi.org/10.1175/jcli3904.1

Wu, W., & Ma, H. Y. (2025). Impacts of resolution on heavy-precipitating storms in climate model Hindcasts. *Journal of Geophysical Research: Atmospheres*, *130*(14), e2024JD042720. https://doi.org/10.1029/2024jd042720

Xie, S.-P. (2004). Satellite observations of cool ocean–atmosphere interaction. *Bulletin of the American Meteorological Society*, *85*(2), 195–208. https://doi.org/10.1175/bams-85-2-195

Zhang, G. J., & McFarlane, N. A. (1995). Sensitivity of climate simulations to the parameterization of cumulus convection in the Canadian Climate Centre general circulation model. *Atmosphere-Ocean*, *33*(3), 407–446. https://doi.org/10.1080/07055900.1995.9649539

References From the Supporting Information

Gregory, D., & Rowntree, P. (1990). A mass flux convection scheme with representation of cloud ensemble characteristics and stability-dependent closure. *Monthly Weather Review*, *118*(7), 1483–1506. https://doi.org/10.1175/1520-0493(1990)118<1483:amfcsw>2.0.co;2

Guérémy, J. (2011). A continuous buoyancy based convection scheme: One-and three-dimensional validation. *Tellus A: Dynamic Meteorology and Oceanography*, *63*(4), 687–706.

Nordeng, T. E. (1994). Numerical simulations of mesoscale substructures and physical processes within extratropical cyclones. In *The life cycles of extratropical cyclones* (pp. 297–315). Springer.

Piriou, J.-M., Redelsperger, J.-L., Geleyn, J.-F., Lafore, J.-P., & Guichard, F. (2007). An approach for convective parameterization with memory: Separating microphysics and transport in grid-scale equations. *Journal of the Atmospheric Sciences*, *64*(11), 4127–4139. https://doi.org/10.1175/2007jas2144.1